

# An approach to robust ICP initialization

Alexander Kolpakov and Michael Werman

**Abstract**—In this note, we propose an approach for initializing the Iterative Closest Point (ICP) algorithm that allows us to apply ICP to unlabelled point clouds that are related by rigid transformations. We also give bounds on the robustness of our approach to noise. Numerical experiments confirm our theoretical findings.

## I. INTRODUCTION

Point set registration is aligning two point clouds using a rigid transformation. The purpose of finding such a transformation includes merging multiple data sets into a globally consistent coordinate frame, mapping a new measurement to a known data set to identify features, or finding the most similar object in a database, [1].

Typically, 3D point cloud data are obtained from stereo, LiDAR, and RGB-D cameras, while 2D point sets are often extracted from features found in images.

Among the numerous registration methods proposed in the literature, the Iterative Closest Point (ICP) algorithm [2], [3], [4], introduced in the early 1990s, is the main algorithm for registering two 2D or 3D point sets using a rigid transformation.

The Iterative Closest Point algorithm contrasts with the Kabsch [5] algorithm and other solutions to the orthogonal Procrustes problem in that the Kabsch algorithm requires a correspondence between the point sets as input, whereas ICP treats correspondence as a variable to be estimated, labeled vs. unlabeled.

The main ICP steps are:

---

### Algorithm 1 ICP

---

```

while not termination condition do
    Find a partial mapping between the sets
    Estimate the transformation based on the previous step
    Transform the source points
end while
  
```

---

As this is a highly non-convex problem it can only find a good solution when the point sets are originally close to being aligned.

Yang et al. [6] present a branch-and-bound scheme for searching the entire 3D rigid transformation space, thus guaranteeing a global optimum. An Overview of transformation estimation between point clouds is presented in [7], [8], including optimization-based and deep learning methods which can also be used to initialize the ICP in certain situations.

A. Kolpakov is at the Université de Neuchâtel. This work was funded in part by the Swiss National Science Foundation [grant no. PP00P2-202667]

M. Werman is at The Hebrew University of Jerusalem. This work was funded in part by the Israeli Science Foundation

Several papers [9], [10], [11], propose using local information and not just the points' coordinates to improve the matching.

This paper presents a good, simple, and provably robust approach to preregister point sets so that the ICP algorithm will have a high chance of converging to a good solution.

## II. MAIN ALGORITHM

Given an  $n$  points in  $\mathbb{R}^d$  with at least  $d+1$  of them distinct we represent it as a  $d \times n$  matrix. The matrix is unique up to a permutation of the columns, or equivalently by right multiplication with a permutation matrix.

Let  $O(d)$  denote the orthogonal matrix group acting on  $\mathbb{R}^d$ , and  $\text{Sym}(n)$  the group of  $n \times n$  permutation matrices.

Given a point cloud  $X$  with  $n$  points, let  $b(X)$  denote the barycenter of  $X$ ,

$$b(X) = \frac{1}{n} \sum_{i=1}^n x_i \quad \text{and} \quad \bar{X} = X - \frac{1}{n} X \mathbf{1}_{n \times n} = X - b(X) \mathbf{1}_{1 \times n}$$

the point set translated to be centered at the origin.

Given a point cloud  $X \in \mathbb{R}^{d \times n}$ , let  $E(X)$  denote its inertia ellipsoid,  $E(X) = X X^t \in \mathbb{R}^{d \times d}$ , also known as the covariance matrix. Note that  $E(X)$  is a positive semidefinite matrix for any  $X$ . Generically  $\text{rank } X = d$  and defines an ellipsoid with non-zero principal half-axes. Otherwise, we have a cylinder in  $\mathbb{R}^d$  whose cross-section is a lower-dimensional ellipsoid. However, we shall only consider the generic case when  $\text{rank } X = d$ , and thus the point cloud cannot be placed inside a lower-dimensional subspace of  $\mathbb{R}^d$ . In this case,  $E = E(X) \in \mathbb{R}^{d \times d}$  is a positive definite matrix.

Let  $E \in \mathbb{R}^{d \times d}$  be a positive definite matrix with distinct eigenvalues  $\lambda_1 > \lambda_2 > \dots > \lambda_d > 0$ . Our next observation is that there are only finitely many ways to perform orthogonal diagonalization on  $E$ .

Let  $\Lambda = \text{diag}(\lambda_1, \dots, \lambda_d)$ . Let  $E = U_1 \Lambda U_1^t = U_2 \Lambda U_2^t$ , for two matrices  $U_1, U_2 \in O(d)$ . Then  $U_2^t U_1 \in O(d)$  is a self-isometry of the “canonical” ellipsoid  $E_0$  defined by the equation  $\lambda_1 x_1^2 + \dots + \lambda_d x_d^2 = 1$  having  $\frac{1}{\lambda_1}, \dots, \frac{1}{\lambda_d}$  as the lengths of its half-axes. Provided the above condition on  $\lambda$ 's, the only self-isometries of  $E_0$  are reflections in the coordinate hyperplanes and their compositions.

Let  $\text{Ref}(d)$  be the group generated by hyperplane reflections of the form  $x_i \mapsto -x_i$  for some  $i \in \{1, 2, \dots, d\}$ ,  $x_j \mapsto x_j$ , for  $j \neq i$ , for all  $i = 1, 2, \dots, d$ . Note that  $\text{Ref}(d)$  is a finite group with  $2^d$  elements. It consists of diagonal matrices with  $+1$ 's and  $-1$ 's on the diagonal.

Thus, if  $E$  can be brought to the same diagonal form by using two orthogonal matrices  $U_1, U_2 \in O(d)$ , then  $U_1^t U_2 \in \text{Ref}(d)$ . This means that there are no more than  $2^d$  ways to diagonalize  $E$  using orthogonal matrices.

Assume that two point clouds  $P, Q \in \mathbb{R}^{d \times n}$  are related by a distance-preserving transformation, that is  $Q$  is obtained from

$P$  by applying an orthogonal transformation followed by a translation.

Let  $O \in O(d)$  be an orthogonal transformation, and  $S \in \text{Sym}(n)$  a permutation matrix. For any point cloud  $X \in \mathbb{R}^{d \times n}$  we have  $b(OX) = O b(X)$  and  $b(XS) = b(X)$ .

Given a point cloud  $X \in \mathbb{R}^{d \times n}$  we also assume that  $\text{rank } X = d$  and  $E(X)$  has all distinct eigenvalues. This assumption is generically true, and can always be achieved by a small perturbation of the points in  $X$ .

As noted by many, when minimizing the least square distance between point sets their barycenters should be aligned, following from:

$$\frac{\partial \sum_{i=1}^n \|Ox_i + b - y_i\|^2}{\partial b} = 0 \Rightarrow b = \frac{1}{n} \sum_{i=1}^n y_i - \frac{1}{n} \sum_{i=1}^n Ox_i$$

Thus, we may assume that  $P$  and  $Q$  are replaced with  $\bar{P}$  and  $\bar{Q}$ , accordingly. Then  $Q = OPS$ , for an orthogonal transformation  $O \in O(d)$  and a permutation matrix  $S \in \text{Sym}(n)$ .

Moreover, we have that  $E_Q = O E_P O^t$  independent of the permutation  $S$ ,  $S^{-1} = S^t$ . This also means that  $E_P$  and  $E_Q$  have the same set of eigenvalues, which are distinct by the previous assumption.

We shall use the following Algorithm for ICP initialization.

---

**Algorithm 2** Initialization

---

$P \leftarrow \bar{P}, Q \leftarrow \bar{Q}$	▷ centering
$E_P \leftarrow P P^t, E_Q \leftarrow Q Q^t.$	
$E_P \leftarrow U_P \Lambda U_P^t, E_Q \leftarrow U_Q \Lambda U_Q^t$	▷ diagonalization
$U_0 \leftarrow U_Q U_P^t$	
$D^* \leftarrow \underset{D \in \text{Ref}(d)}{\text{argmin}} \text{Match}(P, (U_0 U_P D U_P^t)^t Q)$	
$Q \leftarrow (U_0 U_P D^* U_P^t)^t Q$	

---

After initialization, run ICP on  $P$  and  $Q$ .

### III. CORRECTNESS OF THE ALGORITHM

Under the ideal conditions, our Algorithm produces at Step 4 two matrices  $U \in O(d)$  and  $M \in \text{Sym}(n)$  such that  $Q = UPM$ . Even in this case, there is an obstacle to recovering the initial  $O$  and  $S$ . Namely, the cloud  $P$  (and thus  $Q$ ) may have symmetries: an orthogonal transformation  $O' \in O(d)$  is a symmetry of a point cloud  $X \in \mathbb{R}^{d \times n}$  if there exists a permutation  $S' \in \text{Sym}(n)$  such that  $O'X = XS'$ . Then  $U = OO'$ ,  $M = (S')^t S$  will also be a perfect matching of the points of  $P$  to the points of  $Q$ .

In what follows we assume that  $P$  and  $Q$  have no symmetries, which can be achieved generically by a slight perturbation of the respective cloud points. This assumption is not restrictive: in the presence of symmetries, we will have multiple solutions, each of which is as good as any other.

The previous discussion was for *exact* alignment of *equal* sized point sets, the following sections show that both these restrictions can be relaxed.

### IV. ROBUSTNESS TO NOISE

#### A. Multiplicative noise

We first consider multiplicative noise. Noise of this type changes its magnitude depending on the size of point clouds. One natural example is *relative* measurement errors.

Let  $N \in \mathbb{R}^{d \times n}$  be a matrix with entries  $N_{ij} \sim \mathcal{N}(1, \sigma^2)$ ,  $i = 1, \dots, d$ ,  $j = 1, \dots, n$ , independent Gaussian random variables and  $\odot$  denote the Hadamard (elementwise) product of matrices. We shall model a noisy point cloud  $Q = OPS$  by masking  $Q$  with  $N$ , i.e. replacing  $Q$  with  $Q' = Q \odot N$ . In this case, we have that  $\mathbb{E}[Q'] = Q$  and, moreover, if  $b(Q) = 0$  then  $\mathbb{E}[b(Q')] = 0$ , too.

Let  $\mathbb{E}_{Q'} = \mathbb{E}[E(Q')] = \mathbb{E}[E(Q \odot N)]$ ,  $E_{Q'} = E(Q') = E(Q \odot N)$  and  $E_Q = E(Q)$  be the corresponding ellipsoids: the first being the “average ellipsoid” (averaged over the noise,  $N$ ), the second being the “noisy” one, and the third being the “ideal” one.

First we compare  $\mathbb{E}_{Q'}$  to  $E_Q$ . By a straightforward computation, we obtain that

$$\begin{aligned} \mathbb{E}_{Q'} &= \mathbb{E}[(Q \odot N)(Q \odot N)^t] = (Q Q^t) \odot (\mathbf{1}_d \mathbf{1}_d^t + \Sigma) \\ &= E_Q + \sigma^2 \text{diag } E_Q, \end{aligned} \quad (1)$$

where  $\Sigma = \text{diag}(\sigma^2, \dots, \sigma^2)$ .

Thus,

$$\|\mathbb{E}_{Q'} - E_Q\|_2 = \sigma^2 \max_{i=1}^d E_{ii} \leq \sigma^2 \|E_Q\|_2. \quad (2)$$

In particular, this means that the “average” ellipsoid  $\mathbb{E}_{Q'}$  does not deviate from  $E_Q$  too much if the relative noise is small enough.

The above applies to any noise matrix  $N = (N_{ij}) \in \mathbb{R}^{d \times n}$  where the entries  $N_{ij}$  are i.i.d. random variables with  $\mathbb{E}[N_{ij}] = 1$  and  $\text{Var}[N_{ij}] = \sigma^2$ .

By using the analog of Chebyshev’s inequality for symmetric positive definite matrices (see [12, Theorem 14])

$$\mathbb{P}(\|E_{Q'} - \mathbb{E}_{Q'}\|_2 > \delta) \leq \frac{\text{tr } S^2}{\delta^2} \quad (3)$$

where  $S^2 = \mathbb{E}[(E_{Q'})^2] - (\mathbb{E}[E_{Q'}])^2$  is the variance matrix (computed elementwise) and  $\delta > 0$  is a constant.

We have that

$$\text{tr } \mathbb{E}[(E_{Q'})^2] = \mathbb{E}[\text{tr } (E_{Q'})^2] \leq \mu'_4 \text{tr } E_Q^2 \quad (4)$$

where the inequality is obtained by assuming that  $N = (N_{ij}) \in \mathbb{R}^{d \times n}$  has independent entries and  $\mu'_4 \geq \mu'_3 \mu'_1$ ,  $\mu'_4 \geq (\mu'_2)^2$ , where  $\mu'_l$  is the  $l$ -th (non-central) moment of  $\mathcal{N}(1, \sigma^2)$ , i.e.  $\mu'_1 = 1$ ,  $\mu'_2 = 1 + \sigma^2$ ,  $\mu'_3 = 1 + 3\sigma^2$ ,  $\mu'_4 = 1 + 6\sigma^2 + 3\sigma^4$ .

Also, we have

$$\text{tr } (\mathbb{E}[E_{Q'}])^2 = \text{tr } (E_Q + \sigma^2 \text{diag } E_Q)^2 = \text{tr } (E_Q^2) + 2\sigma^2 \Delta + \sigma^4 \Delta, \quad (5)$$

where  $\Delta = \sum_{i=1}^d E_{ii}^2$ .

Then we estimate  $\text{tr } S^2$  by combining Eq. 4 and Eq. 5 as follows:

$$\begin{aligned} \text{tr } S^2 &= \text{tr } \mathbb{E}[(E_{Q'})^2] - \text{tr } (\mathbb{E}[E_{Q'}])^2 \\ &\leq \sigma^2 (2 + \sigma^2) (3 \text{tr } E_Q^2 - \Delta) \\ &\leq 9d \sigma^2 \|E_Q\|_2^2, \end{aligned} \quad (6)$$

as we assume  $\sigma \leq 1$ .

Finally, by combining Eq. 3 with Eq. 6, we obtain

$$\mathbb{P}(\|E_{Q'} - \mathbb{E}_{Q'}\|_2 > \delta) \leq \frac{9 d \sigma^2 \|E_Q\|_2^2}{\delta^2}. \quad (7)$$

Setting  $\delta = \varepsilon \|E_Q\|_2$  in Eq. 7

$$\mathbb{P}(\|E_{Q'} - \mathbb{E}_{Q'}\|_2 > \varepsilon \|E_Q\|_2) \leq d \left( \frac{3\sigma}{\varepsilon} \right)^2, \quad (8)$$

for any fixed  $\varepsilon > 0$ . In this instance we can fulfill the usual “three-sigma” rule by choosing  $\varepsilon = \sqrt{3d\sigma}$ .

Thus, Eq. 2 and Eq. 8 imply that with probability  $1 - \Omega(\sigma)$  we have that

$$\|E_{Q'} - E_Q\|_2 \leq \|E_{Q'} - \tilde{E}_Q\|_2 + \|\tilde{E}_Q - E_Q\|_2 \leq (\sqrt{3d\sigma} + \sigma^2) \|E_Q\|_2 = (\sqrt{3d\sigma} + o(\sigma)) \|E_Q\|_2. \quad (9)$$

Note that above we measure the magnitude of the scale-invariant quantity  $\frac{\|E_{Q'} - E_Q\|_2}{\|E_Q\|_2}$  that corresponds to the relative difference of the ellipsoids. Indeed, simultaneous scaling of the point clouds by some non-zero factor would also induce scaling of the ellipsoids. However, this should not affect the orthogonal transformations or the point matching between the clouds.

Recall that  $E_{Q'} = U P, M$  for some  $U \in O(d)$  and  $M \in \text{Sym}(n)$ , while  $E_Q = O P S$  for some  $O \in O(d)$  and  $S \in \text{Sym}(n)$ . By setting  $E_P = E(P)$ , as before, we get

$$\|E_P - U^t O E_P O^t U\|_2 = \|U E_P U^t - O E_P O^t\|_2 = \|E_{Q'} - E_Q\|_2 \leq (\sqrt{3d\sigma} + o(\sigma)) \|E_Q\|_2. \quad (10)$$

Since  $\|E_Q\|_2 = \|E_P\|_2$ , we can rewrite the above as

$$\|\hat{E}_P - U^t O \hat{E}_P O^t U\|_2 \leq \sqrt{3d\sigma} + o(\sigma), \quad (11)$$

where  $\hat{E}_P = \frac{E_P}{\|E_P\|_2}$  is the “normalized” ellipsoid. As remarked above, such normalization does not affect our analysis of the proximity of  $Q$  and  $U$ .

Once  $\|\hat{E}_P - W \hat{E}_P W^t\|_2 = 0$  for some  $W \in O(d)$  we have  $W \hat{E}_P = \hat{E}_P W$ . Up to a change of basis we may assume that  $E_P = \Lambda = \text{diag}(\lambda_1, \dots, \lambda_d)$  with  $\lambda_1 > \lambda_2 > \dots > \lambda_d > 0$  all distinct, as before. Then  $\hat{E}_P = \text{diag}(1, \lambda_1^{-1} \lambda_2, \dots, \lambda_1^{-1} \lambda_n)$ . This implies immediately that  $W$  is diagonal, and thus  $W \in \text{Ref}(d)$ . Since by assumption  $P$  does not have symmetries, we can only have  $W$  being the identity transformation  $I_d$ .

Thus, if  $\varepsilon$  and  $\sigma$  in Eq. 11 are small enough, we have  $U^t O$  is close to  $I_d$ , and thus  $U$  that matches the initial cloud  $P$  to the noisy cloud  $Q'$  will approximate well the genuine transformation  $O$  that matches  $P$  exactly to  $Q$ .

### B. Additive noise

Additive noise is also present under usual circumstances. One example is the background noise in the communication channel.

In this case, let  $N \in \mathbb{R}^{d \times n}$  be a matrix with entries  $N_{ij} \sim \mathcal{N}(0, \sigma^2)$ ,  $i = 1, \dots, d$ ,  $j = 1, \dots, n$ , independent Gaussian random variables. To model noise, we replace  $Q$  with  $Q' = Q + N$ . As before,  $\mathbb{E}[Q'] = Q$ . Moreover, once  $b(Q) = 0$ , then  $\mathbb{E}[b(Q')] = 0$ , too.

Let  $\xi = \|E_{Q'} - E_Q\|_F$  be the non-negative random variable measuring the difference between the “noisy” ellipsoid  $E_{Q'}$  and the “ideal” ellipsoid  $E_Q$ . Here we prefer to use the Frobenius norm instead of the spectral radius, although these norms are equivalent and our choice is only that of convenience.

First, we compute

$$E_{Q'} = (Q + N)(Q + N)^t = E_Q + Q N^t + N Q^t + N N^t, \quad (12)$$

and thus

$$\xi = \|E_{Q'} - E_Q\|_F \leq 2 \|Q\|_F \|N\|_F + \|N\|_F^2, \quad (13)$$

by subadditivity and submultiplicativity of the Frobenius norm.

By using  $\mathbb{E}[\sqrt{\eta}] \leq \sqrt{\mathbb{E}[\eta]}$  for any non-negative random variable, we obtain

$$\mathbb{E}[\xi] \leq 2 \|Q\|_F \sqrt{\mathbb{E}[\|N\|_F^2]} + \mathbb{E}[\|N\|_F^2] = 2 \|Q\|_F \sqrt{nd\sigma} + nd\sigma^2. \quad (14)$$

By using  $\|X + Y\|_F^2 \leq 2 \|X\|_F^2 + 2 \|Y\|_F^2$  for any  $X, Y \in \mathbb{R}^{d \times d}$ , we get

$$\xi^2 = \|Q N^t + N Q^t + N N^t\|_F^2 \leq 8 \|Q\|_F^2 \|N\|_F^2 + 2 \|N\|_F^4. \quad (15)$$

Here we also use submultiplicativity of the Frobenius norm.

As noted before  $\mathbb{E}[\|N\|_F^2] = nd\sigma^2$ . Also, we have  $\mathbb{E}[\|N\|_F^4] \leq n^2 d^2 \mu_4$ , where  $\mu_i$  is the  $i$ -th central moment of  $\mathcal{N}(0, \sigma^2)$ . The latter inequality follows from  $\mu_4 = 3\sigma^4 > \sigma^4 = \mu_2^2$ . Thus

$$\mathbb{E}[\xi^2] \leq 8 \|Q\|_F^2 nd\sigma^2 + 6 n^2 d^2 \sigma^4. \quad (16)$$

Let  $\delta > 0$  be a positive real number. Then the classical Markov inequality implies

$$\mathbb{P}(\|E_{Q'} - E_Q\|_F > \delta) \leq \frac{\mathbb{E}[\xi^2]}{\delta^2}, \quad (17)$$

where  $E_Q = O E_P O^t$  and  $E_{Q'} = U E_P U^t$ , for some  $U \in O(d)$ .

By setting  $\delta = \sqrt{3\sigma} \|Q\|_F$  in Eq. (17) and using Eq. (16) we compute

$$\begin{aligned} & \mathbb{P}(\|E_{Q'} - E_Q\|_F > \sqrt{3\sigma} \|Q\|_F) \\ & \leq \frac{8 nd\sigma^2 \|Q\|_F^2}{3\sigma \|Q\|_F^2} + \frac{6 n^2 d^2 \sigma^4}{3\sigma \|Q\|_F^2} \leq 3 nd\sigma + o(\sigma). \end{aligned} \quad (18)$$

Let  $\tilde{E}_P = \frac{E_P}{\|P\|_F^2}$  be the “normalized” ellipsoid. By using Eq. (16) together with the fact that  $\|Q\|_F = \|P\|_F$  we obtain

$$\|\tilde{E}_P - U^t O \tilde{E}_P O^t U\|_F \leq \sqrt{3\sigma} \quad (19)$$

may fail with probability not exceeding  $3 nd\sigma + o(\sigma)$ , which is reasonably small for small values of  $\sigma$ .

By using Eq. 19 and applying an analogous argument as in Subsection IV-A, we obtain that for sufficiently small  $\sigma$   $O$  is close to the identity transformation  $I_d$ . Thus, the recovered transformation  $U$  that matches the initial cloud  $P$  to the noisy cloud  $Q'$  will approximate  $O$  well enough.

## V. NUMBER OF POINTS DISCREPANCY

Now let  $Q = OPS$ , for a point cloud  $P \in \mathbb{R}^{d \times k}$ , an orthogonal transformation  $O \in O(d)$  and a permutation matrix  $S \in \text{Sym}(k)$  but in this case, we are given  $P' \supset P$  and  $Q' \supset Q$ .

Thus, we assume that the two point clouds  $P'$  and  $Q'$  can be partially matched by using ICP despite likely having different cardinality. We need to understand how the norms of  $\Delta P = P' \setminus P$  and  $\Delta Q = Q' \setminus Q$  may affect our approach.

Let  $E_{P'} = E(P')$ ,  $E_{Q'} = E(Q')$ ,  $E_{\Delta P} = E(\Delta P)$ , and  $E_{\Delta Q} = E(\Delta Q)$ . A straightforward computation shows that  $E_{P'} = E_P + E_{\Delta P}$  and  $E_{Q'} = E_Q + E_{\Delta Q}$ .

Let  $U_0 \in O(d)$  be obtained by running Steps 1,2, and 3 of the Algorithm with  $P'$  and  $Q'$  as input: we have  $E_{Q'} = U_0 E_{P'} U_0^t$ .

Note that we also have  $E_Q = O E_P O^t$ . Thus, we get

$$U_0 E_P U_0^t - O E_P O^t = U_0 E_{\Delta P} U_0^t - E_{\Delta Q} \quad (20)$$

that implies

$$\begin{aligned} \|E_P - U_0^t O E_P O^t U_0\|_2 &= \|U_0 E_{\Delta P} U_0^t - E_{\Delta Q}\|_2 \\ &\leq \|E_{\Delta P}\|_2 + \|E_{\Delta Q}\|_2. \end{aligned} \quad (21)$$

Assume that  $\|E_{\Delta P}\|_F \leq \frac{\varepsilon}{2\sqrt{d}} \|E_P\|_F$  and  $\|E_{\Delta Q}\|_F \leq \frac{\varepsilon}{2\sqrt{d}} \|E_Q\|_F$ . This will be the case, e.g. when the norm of vectors in  $P$  and  $\Delta P$  are relatively comparable while  $P$  contains considerably more points than  $\Delta P$  and the same holds for  $Q$  and  $\Delta Q$ .

For any non-degenerate matrix  $X \in \mathbb{R}^{d \times d}$  we have  $\|X\|_2 \leq \|X\|_F \leq \sqrt{d} \|X\|_2$  between its Frobenius norm  $\|X\|_F$  and its spectral radius  $\|X\|_2$ . Thus we get

$$\|E_P - U_0^t O E_P O^t U_0\|_2 \leq \frac{\varepsilon}{2} (\|E_P\|_2 + \|E_Q\|_2) \leq \varepsilon \|E_P\|_2. \quad (22)$$

As before, for the normalised ellipsoid  $\hat{E}_P$  we obtain

$$\|\hat{E}_P - U_0^t O \hat{E}_P O^t U_0\|_2 \leq \varepsilon. \quad (23)$$

Once  $\varepsilon$  is small enough, the same logic as in Section IV leads to the conclusion that, up to a change of basis, we have  $U_0 = OD$  for an element  $D \in \text{Ref}(d)$ . Since in Step 4 of the Algorithm each element of  $\text{Ref}(d)$  is tested, we still shall obtain the best match starting with  $U_0$ . The rest of the algorithm will then work out as usual.

Thus, the transformation  $O \in O(d)$  and the point matching  $S \in \text{Sym}(k)$  still will be recovered once we initialize ICP to match two considerably large parts of  $P \in \mathbb{R}^{d \times k}$  of a point cloud  $P' \in \mathbb{R}^{d \times m}$  and  $Q = OPS \in \mathbb{R}^{d \times k}$  of a point cloud  $Q' \in \mathbb{R}^{d \times n}$ .

## VI. SUPERPOSITION OF ERRORS

If several of the above issues (multiplicative or additive noise, or point cardinality discrepancy) are present, then the errors will add up according to the triangle inequality for matrix norms. If all three kinds of errors are relatively small, our Algorithm will have enough robustness.

## VII. POSSIBLE MODIFICATIONS

The Algorithm is based on aligning the eigenvectors (principal half-axes) of two ellipsoids associated with the respective points clouds. In the above, eigenvectors are matched based on the order of eigenvalues. However, in the case of excessive noise, some eigenvalues may switch. To tackle this issue, instead of treating the uncertainty in ellipsoid matching as an element of  $\text{Ref}(d)$ , we assume that we can be wrong up to a bigger finite group: the  $2^d d!$  element  $B_d$  Coxeter group that also permutes the coordinate axes.

## VIII. NUMERICAL EXPERIMENTS

### A. Main algorithm: random point clouds

100 tests were executed. Each time a random point cloud  $P \subset \mathbb{R}^3$  with 100 points is generated. The points in  $P$  are distributed uniformly in the cube  $[-20, 20]^3$  (each coordinate being uniformly distributed). Then a random orthogonal matrix  $O \in O(3)$  and a random permutation  $S \in \text{Sym}(100)$  are generated, and the cloud  $Q = OPS$  is produced. In all tests, ICP initialized with our algorithm recovered  $O$  and  $S$  (up to machine precision). In fact, we only need to run ICP to recover the nearest neighbors, and thus the permutation  $S$ . The initial orthogonal transformation  $U = U_0 U_P D^* U_P^t$  from the initialization Algorithm is already equal to  $O$  under ideal conditions.

### B. Main algorithm: Caerbannog point clouds

100 tests as described above were performed on each of the three unoccluded Caerbannog clouds [13]: the teapot, the bunny<sup>1</sup>, and the cow. All tests successfully recovered both  $O$  and  $S$ .

### C. Main algorithm: comparison to ICP without initialization

We compare ICP initialized with our Algorithm to ICP without initialization in the case of the Caerbannog clouds described above. In a batch of 100 tests, we obtained (under ideal conditions) a 100% failure rate without initialization, and 100% success rate for ICP initialized with our algorithm.

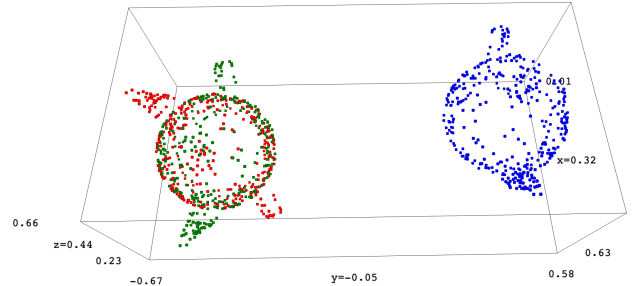


Fig. 1. A typical result of ICP applied to the “teapot” cloud without initialization: the initial cloud  $P$  (blue), the image  $Q$  (red) of  $P$  under an orthogonal transformation, and the image of  $P$  recovered by ICP (green).

<sup>1</sup>Also known as the Killer Rabbit of Caerbannog.

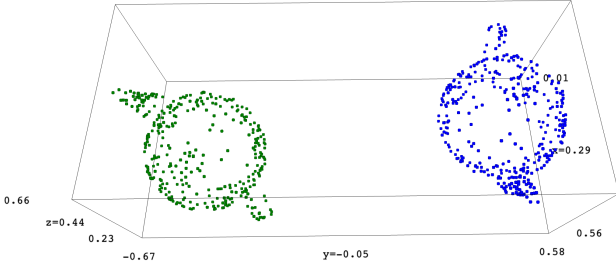


Fig. 2. A typical result ICP applied to the “teapot” cloud with initialization. The initial cloud  $P$  is plotted in blue, while the image  $Q$  of  $P$  under an orthogonal transformation is plotted in red, and the image of  $P$  recovered by ICP is plotted in green. However, the green and red images completely overlap.

#### D. Multiplicative noise

100 tests were performed on each of the three unoccluded Caerbannog clouds [13]: the teapot, the bunny, and the cow. All tests were successful in recovering  $O$  with relatively minor errors given that the noise is also relatively minor. Recovering the permutation  $S$  fails in most cases as even relatively minor noise interferes seriously with the nearest neighbors matching.

In each test, we obtain an orthogonal transformation  $U_{init}$  from our initialization algorithm, and then further an improved transformation  $U_{icp}$  after running ICP. We also obtain the image of  $P$  from ICP, i.e.  $Q_{icp} = U_{icp} P S_{icp}$ , and can compare it to  $Q'$  after matching the nearest neighbors of  $Q_{icp}$  and  $Q'$  by using a matching matrix  $S_{icp}$ . We can also compare  $Q_{icp}$  to the actual specimen image  $Q = O P S$  of  $P$ .

We also find it instructive to compute the improvement that ICP makes to the initializing orthogonal transformation  $U$ , as well as the distance between  $Q_{init} = U P S_{icp}$  and  $Q_{icp}$ .

In all tests, we used Gaussian (multiplicative) noise with  $\mu = 1$  and  $\sigma = 0.07$ . The following values were measured:

- the added noise (normalized):  $\nu = \|Q' - Q\|_2 / \|P\|_2$ ;
- the normalized distance to the noisy image  $Q'$ :  $\delta = \|Q' - Q_{icp}\|_2 / \|P\|_2$ ;
- the normalized distance to the actual (without noise) specimen image:  $\delta_{spec} = \|Q - Q_{icp} S_{icp}^t S\|_2 / \|P\|_2$ ;
- the distance to the initial orthogonal transformation  $\delta_o = \|U_{icp} - O\|_2$ ;
- the normalized Hamming distance to the initial permutation  $\delta_H = \|S_{icp} - S\|_F / (4 \cdot n)$ ;
- the ICP improvement in the (normalised) distance  $\delta^{icp} = \|Q_{init} - Q_{icp}\|_2 / \|P\|_2$ ;
- the ICP change to the initial orthogonal transformation:  $\delta_o^{icp} = \|U_{init} - U_{icp}\|_2 / \|P\|_2$ .

In all our tests we choose  $\delta_{spec} < 0.05$  as the success criterion. In Fig. 3 we plot the success rate depending on the added noise  $\nu$ .

Judging from Fig. 3, most tests fail for  $\nu > 0.3$  (which also corresponds to  $\sigma^2 > 0.3$ ).

We also produce the plots for  $\delta_{spec}$  (Fig. 4) and  $\delta_o$  (Fig. 5) depending on  $\nu$ . In Fig. 6 the case of a noisy “teapot” cloud is shown.

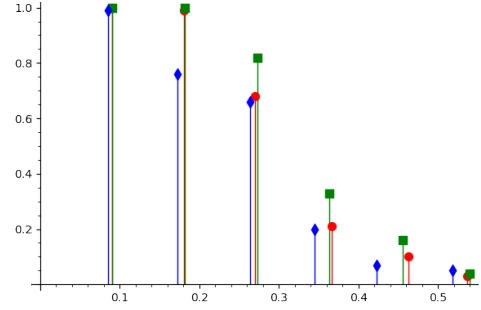


Fig. 3. Success rate  $\tau$  (vertical axis) depending on the normalised multiplicative noise  $\eta$  (horizontal axis) measured over 100 tests for each of the “teapot” (red circle), “bunny” (green square) and “cow” (blue lozenge) point clouds. The measurements of  $(\nu, \tau)$  are performed for Gaussian multiplicative noise  $\mathcal{N}(1, \sigma^2)$  with  $\sigma^2$  taking consecutive values 0.1, 0.2, ..., 0.6.

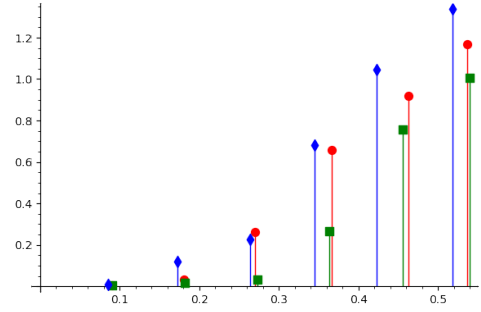


Fig. 4. Normalized distance to the specimen  $\delta_{spec}$  (vertical axis) depending on the normalised multiplicative noise  $\eta$  (horizontal axis) measured over 100 tests for each of the “teapot” (red circle), “bunny” (green square) and “cow” (blue lozenge) point clouds. The measurements of  $(\nu, \delta_{spec})$  are performed for Gaussian multiplicative noise  $\mathcal{N}(1, \sigma^2)$  with  $\sigma^2$  taking consecutive values 0.1, 0.2, ..., 0.6.

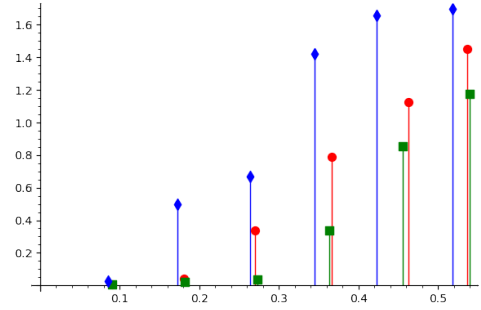


Fig. 5. Distance to the initial orthogonal transformation  $\delta_o$  (vertical axis) depending on the normalised multiplicative noise  $\eta$  (horizontal axis) measured over 100 tests for each of the “teapot” (red circle), “bunny” (green square) and “cow” (blue lozenge) point clouds. The measurements of  $(\nu, \delta_o)$  are performed for Gaussian multiplicative noise  $\mathcal{N}(1, \sigma^2)$  with  $\sigma^2$  taking consecutive values 0.1, 0.2, ..., 0.6.

#### E. Additive noise

100 tests, as described above were performed on each of the three unoccluded Caerbannog clouds [13]: the teapot, the bunny, and the cow. The procedure and measurements were similar to the case of multiplicative noise.

In Fig. 7 we plot the success rates measured for different levels of noise by running 100 tests in each case, for each of the Caerbannog clouds.

In Fig. 8 the case of a noisy “bunny” cloud is shown.

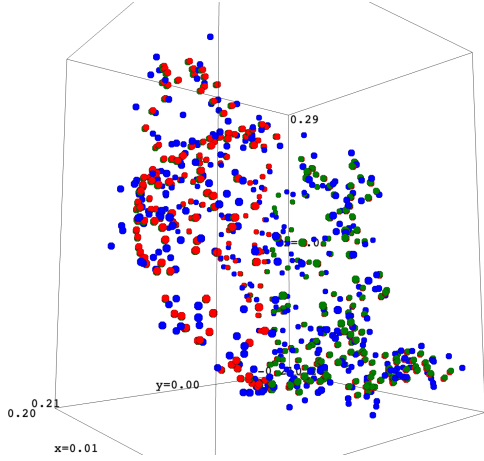


Fig. 6. Multiplicative noise with  $\nu = 0.087$  ( $\sigma^2 = 0.1$ ) on the “teapot” cloud. Shown in the plot is the specimen cloud  $Q$  (red), the noisy cloud  $Q'$  (blue) and the recovered cloud  $Q_{icp}$  (green). There is a significant overlap between the point clouds.

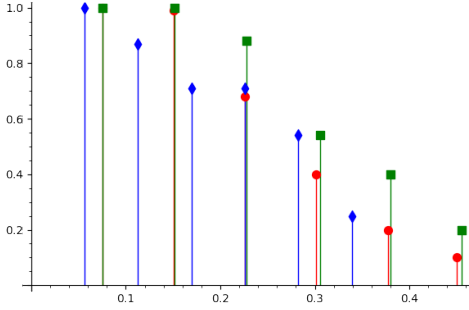


Fig. 7. Success rate  $\tau$  (vertical axis) depending on the normalised additive noise  $\eta$  (horizontal axis) measured over 100 tests for each of the “teapot” (red circle), “bunny” (green square) and “cow” (blue lozenge) point clouds. The measurements of  $(\nu, \tau)$  are performed for Gaussian multiplicative noise  $\mathcal{N}(0, \sigma^2)$  with  $\sigma^2$  taking consecutive values  $0.01, 0.02, \dots, 0.06$ .

Additional plots and test statistics are publicly available from the GitHub repository.

### F. Occluded images

A batch of 100 tests as described above was performed on each of the three unoccluded Caerbannog clouds [13]: the teapot, the bunny, and the cow. We used  $P' = P$  unoccluded as a specimen cloud, and  $Q' = Q \cup \Delta Q$  as its occluded image. Here  $Q = OPS$ , as described in Section V, and  $\Delta Q$  was created as follows. First, we determine the rectangular bounding box  $B$  for  $Q$  with sides parallel to the coordinate planes, and then generate uniformly inside  $B$  random points  $\Delta Q$ . The cardinality of  $\Delta Q$  is controlled by the level of occlusion  $\alpha$ : namely  $|\Delta Q|$  is the integer part of  $\alpha|Q|$ .

In all tests, we used  $\alpha = 0.25$  and measured the following values.

- the added occlusion (normalized):  $\nu = \|Q' - Q\|_2 / \|P\|_2$ ;
- the normalized distance to the occluded image  $Q'$ :  $\delta = \|Q' - Q_{icp}\|_2 / \|P\|_2$ ;
- the normalized distance to the actual specimen image:  $\delta_{spec} = \|Q - Q_{icp} S_{icp}^t S\|_2 / \|P\|_2$ ;

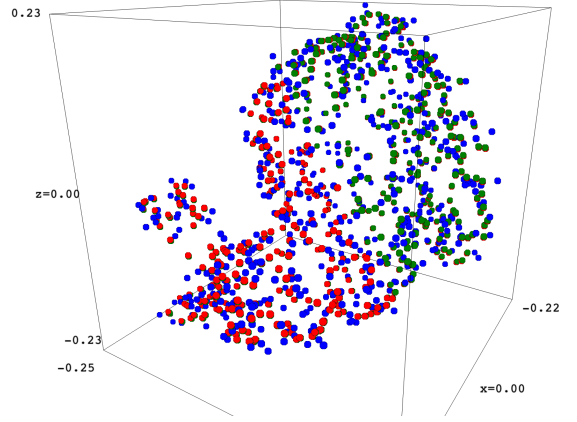


Fig. 8. Additive noise with  $\nu = 0.074$  ( $\sigma^2 = 0.01$ ) on the “bunny” cloud. Shown in the plot is the specimen cloud  $Q$  (red), the noisy cloud  $Q'$  (blue) and the recovered cloud  $Q_{icp}$  (green). There is a significant overlap between the point clouds.

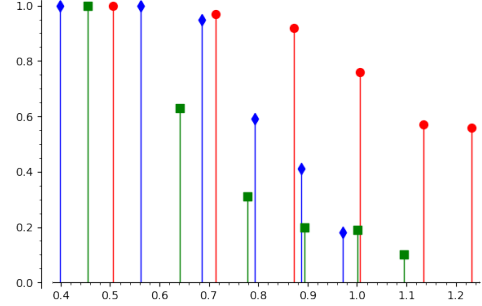


Fig. 9. Success rate  $\tau$  (vertical axis) depending on the normalised occlusion  $\eta$  (horizontal axis) measured over 100 tests for each of the “teapot” (red circle), “bunny” (green square) and “cow” (blue lozenge) point clouds. The measurements of  $(\nu, \tau)$  are performed for occlusion levels of  $\alpha = 0.2, 0.4, \dots, 1.2$ .

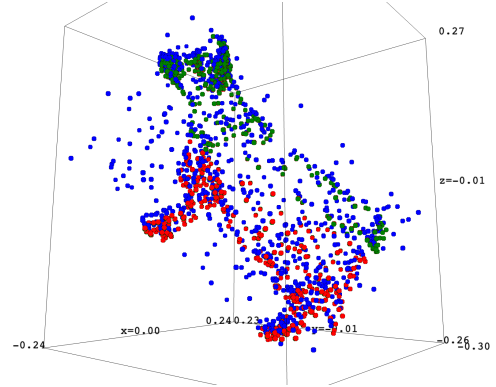


Fig. 10. Occlusion with  $\nu = 0.572$  ( $\alpha = 0.4$ ) on the “cow” cloud. Shown in the plot is the specimen cloud  $Q$  (red), the occluded cloud  $Q'$  (blue), and the recovered cloud  $Q_{icp}$  (green). There is a significant overlap between the point clouds.

- the distance to the initial orthogonal transformation  $\delta_o = \|U_{icp} - O\|_2$ ;
- the ICP improvement in the (normalised) distance  $\delta_{icp} = \|Q_{init} - Q_{icp}\|_2 / \|P\|_2$ ;
- the ICP change to the initial orthogonal transformation:  $\delta_o^{icp} = \|U_{init} - U_{icp}\|_2 / \|P\|_2$ .

In Fig. 9 we plot the success rates measured for different levels of noise by running 100 tests in each case, for each of



the Caerbannog clouds.

In Fig. 10 the case of a noisy “cow” cloud is shown. Additional plots are publicly available from the GitHub repository.

### G. GitHub repository

The SageMath code used to perform the numerical experiments described above is available for download on GitHub at <https://github.com/sashakolpakov/icp-init>. The open course computer algebra system SageMath (freely available at <https://www.sagemath.org/>) is required to run the code.

## REFERENCES

- [1] Wikipedia contributors, “Point-set registration — Wikipedia, the free encyclopedia,” 2022. [Online]. Available: [https://en.wikipedia.org/w/index.php?title=Point-set\\_registration&oldid=1096186590](https://en.wikipedia.org/w/index.php?title=Point-set_registration&oldid=1096186590)
- [2] P. Besl and N. D. McKay, “A method for registration of 3-D shapes,” *IEEE Transactions on Pattern Analysis and Machine Intelligence*, vol. 14, no. 2, pp. 239–256, 1992.
- [3] Y. Chen and G. Medioni, “Object modeling by registration of multiple range images,” in *Proceedings. 1991 IEEE International Conference on Robotics and Automation*, 1991, pp. 2724–2729 vol.3.
- [4] Wikipedia contributors, “Iterative closest point — Wikipedia, the free encyclopedia,” 2022. [Online]. Available: [https://en.wikipedia.org/w/index.php?title=Iterative\\_closest\\_point&oldid=1095051621](https://en.wikipedia.org/w/index.php?title=Iterative_closest_point&oldid=1095051621)
- [5] W. Kabsch, “A solution for the best rotation to relate two sets of vectors,” *Acta Crystallographica Section A*, vol. 32, no. 5, pp. 922–923, 1976. [Online]. Available: <https://doi.org/10.1107/S0567739476001873>
- [6] J. Yang, H. Li, D. Campbell, and Y. Jia, “Go-icp: A globally optimal solution to 3D ICP point-set registration,” *IEEE transactions on pattern analysis and machine intelligence*, vol. 38, no. 11, pp. 2241–2254, 2015.
- [7] X. Huang, G. Mei, J. Zhang, and R. Abbas, “A comprehensive survey on point cloud registration,” *arXiv preprint arXiv:2103.02690*, 2021.
- [8] H. Si, J. Qiu, and Y. Li, “A review of point cloud registration algorithms for laser scanners: Applications in large-scale aircraft measurement,” *Applied Sciences*, vol. 12, no. 20, 2022. [Online]. Available: <https://www.mdpi.com/2076-3417/12/20/10247>
- [9] J. Serafin and G. Grisetti, “Nlcp: Dense normal based point cloud registration,” in *2015 IEEE/RSJ International Conference on Intelligent Robots and Systems (IROS)*. IEEE, 2015, pp. 742–749.
- [10] —, “Using extended measurements and scene merging for efficient and robust point cloud registration,” *Robotics and Autonomous Systems*, vol. 92, pp. 91–106, 2017.
- [11] A. Makovetskii, S. Voronin, V. Kober, , and A. Voronin, “A regularized point cloud registration approach for orthogonal transformations,” *Journal of Global Optimization*, 2022.
- [12] R. Ahlswede and A. Winter, “Strong converse for identification via quantum channels,” *IEEE Trans. Inf. Theory*, vol. 48, no. 3, pp. 569–579, 2002. [Addendum *ibid* 49(1):346, 2003].
- [13] S. Raghupathi, N. Brunhart-Lupo, and K. Gruchalla, “Caerbannog point clouds. National renewable energy laboratory,” <https://data.nrel.gov/submissions/153>, 2020.



**Michael Werman** Michael Werman received the Ph.D. degree from The Hebrew University, in 1986, where he is currently a Professor of computer science. His current research interests include designing computer algorithms and mathematical tools for analyzing, understanding, and synthesizing pictures.



**Alexander Kolpakov** Alexander Kolpakov received the Ph.D. degree from the University of Fribourg, Switzerland, in 2013. Currently he is an Assistant Professor at the University of Neuchâtel. His research interests belong to the domains of Riemannian geometry and group theory, and also include applications of geometry to data science and image processing.